Processing and Application of Ceramics 17 [4] (2023) 436–445
https://doi.org/10.2298/PAC2304436W

Enhancing Al_2O_3-7A52 brazed joints by femtosecond laser surface machining of periodic alumina structure

Haifeng Wang, Deku Zhang*, Zhengbiao Wei, Kehong Wang, Xiaopeng Li

School of Material Science and Engineering, Nanjing University of Science and Technology, Nanjing 210094, China

Received 6 September 2023; Received in revised form 6 December 2023; Accepted 14 December 2023

Abstract

In this study, we propose a method that utilizes femtosecond laser surface machining technology to enhance the quality of ceramic-aluminium alloy joints while minimizing residual stress. The present study investigates the impact of the periodic structure of Al_2O_3 surface, which is machined using femtosecond laser, on the properties of Al_2O_3-7A52 brazed joint. Various surface periodic structures, including shallow grooves, deep grooves and micro-convex platform, were created on the surface of Al_2O_3 using femtosecond laser technology. The joint strengths of these different periodic structures are 44.6, 49.1 and 41.1 MPa, respectively, making 129%, 142% and 119% of the shear strength observed in the original planar ceramic-aluminium alloy joint. By machining ceramic surfaces with femtosecond lasers, a periodic structure can be created that enhances the bonding area between the ceramics and solder. This increased surface area improves the wettability of the solder to the ceramic surface, encouraging diffusion reactions at the joint interface. Ultimately, this leads to the creation of a solid bond with the ceramic interface, facilitated by the formation of spinel ($MgAl_2O_4$).

Keywords: *surface machining, femtosecond laser, Al_2O_3 ceramics, Al alloy, wettability, joint strength*

I. Introduction

There are significant disparities in bonding types as well as physical and chemical properties between ceramic materials and aluminium alloy, leading to considerable challenges in achieving a reliable connection between two materials [1]. To begin with, ceramic materials are primarily composed of covalent and ionic bonds, which possess a significant amount of bond energy and stability. As a result, it is challenging to form pairs of lone electrons during the fusion welding process, making it nearly impossible to achieve successful fusion welding of ceramic materials [2,3]. At the same time, it should be noted that ceramics display poor wettability towards aluminium alloys, making it difficult for them to be wetted by molten aluminium. Moreover, the thermodynamic properties of ceramic materials vastly differ from those of aluminium alloys. The linear expansion coefficient of ceramics is approximately one order of magnitude lower than that of aluminium alloys [4,5]. When ceramics and aluminium alloy are joined together through hot pressing, large residual thermal stress can easily arise at the joint. As a result, defects like joint failure and cracking may occur [6]. Brazing offers the possibility of connecting ceramics and aluminium alloy, although it typically necessitates pre-metallization treatment on the surface of the ceramic material.

Ksiazek *et al.* [7] successfully enhanced the wettability of a ceramic substrate at high temperatures by applying a layer of titanium (Ti) and niobium (Nb) film onto the surface of an Al_2O_3 substrate using the physical vapour deposition (PVD) method. Additionally, they were able to fabricate a joint between the ceramic and aluminium alloy materials. The process of ceramic pre-gold attribution can enhance the wettability of ceramics and establish a strong connection between them. However, due to the mechanical occlusion between the metallized layer and the ceramic material, it becomes challenging to meet the strength criteria for engineering applications.

In order to enhance the bonding strength between ceramics and metal, it is imperative to enhance the metal's adhesion to ceramics by improving its wettability, while simultaneously reducing the residual stress between the

* Corresponding authors: tel: +86 13951012239,
e-mail: *zdk@njust.edu.cn*

two materials. An effective method to achieve this has been established by machining the ceramic surface to form a periodic structure [8,9]. As a highly efficient noncontact technology that employs flexible tools, laser precision engineering is a crucial advanced processing technique for producing micro-nanostructures of superior quality. This technique is particularly suited for creating new functional optoelectronic devices and structures [10]. The utilization of micro and nanoscale surface engineering is vital in enhancing the characteristics of materials [11,12]. After laser irradiation, the material surface can easily form a striped arrangement. This structure is influenced by the polarization of the laser's electric field and can be controlled to create a periodic structure known as laser-induced surface periodic structure (LIPSS or ripples) [13–16].

Numerous scholars have discovered that incorporating femtosecond laser technology in the processing of certain refractory materials can facilitate surface pretreatment and enhance the materials' wettability and roughness, thus effectively achieving the desired outcome [17–19]. A study by Vorobyev *et al.* [20] revealed that femtosecond laser technology can be used to create a novel surface pattern on single crystal Si, resulting in a super-wettable surface with enhanced capillary effects. Jagdheesh *et al.* [21] employed ultraviolet pulsed laser technology to produce periodic patterns on the surface of Al_2O_3 ceramics, in order to achieve super hydrophobic surfaces without causing any damage. Chen *et al.* [22] were able to excite the Al layer on the surface of AlN ceramics using femtosecond laser irradiation, resulting in the formation of Al–O bonds in air. This greatly enhanced the hydrophilicity of the ceramic surface, and facilitated the effective connection between ceramics and metals. Chen *et al.* [23] achieved successful fabrication of periodic structures of bumps and grooves on Ti_3SiC_2 ceramics using femtosecond laser. Through the utilization of microstructure, they were able to effectively reduce the wetting angle of solder on the ceramic surface, optimize the interfacial reaction and reduce the formation of brittle intermetallic compounds. Zhang *et al.* [9] utilized femtosecond laser ablation to create microscale periodic surface groove patterns on a ceramic surface. When brazed with AgCuTi solder at high temperatures and vacuum, the joint strength of the ceramic and 304 stainless steel was approximately 2.75 times greater than that of a planar ceramic joint (66 MPa) under the condition of well-designed surface grooves.

This paper presents a method for enhancing the quality of brazed joints in Al_2O_3-7A52 aluminium alloy. We utilized femtosecond laser surface machining technology to produce periodic shallow grooves, deep grooves, and micro-convex platform on the surface of Al_2O_3. The results demonstrated that the periodic ceramic surface structure significantly enhanced the wettability of solder to the ceramic surface and consequently, improved the brazing quality ceramics-aluminium alloy joint.

II. Experimental

In the experiment a highly durable composite armoured aluminium alloy known as 7A52 was utilized. This particular alloy was shaped into $12 \times 12 \times 8$ mm blocks using a precise diamond wire cutting machine. The chemical composition of this alloy can be found in Table 1. In addition, Al_2O_3 ceramics measuring $10 \times 10 \times 5$ mm and brazing material Al-10.5Si-1.5Mg with dimensions of $12 \times 12 \times 0.1$ mm were also used. Before the brazing process, the brazed surface to be welded was polished with #1200 sandpaper, then washed with 10% sodium hydroxide solution at 60 °C for 35–40 s, and finally pickled with 10% nitric acid solution for 20 s to remove the surface oxide film and blow-dry after ultrasonic cleaning. Ultrasonic cleaning of ceramic surface with acetone solution was carried out for 15 min before brazing. After cleaning, the samples were assembled as shown in Fig. 1a.

After welding, the sample was ground to the connection interface between the exposed ceramics and the aluminium alloy with #120 sandpaper, and the joint was smoothened and polished with #400-to-#2000 sandpaper. A Zeiss-stemi 2000 microscope was used to observe the macro-morphology of the metal and ceramics. For the phase analysis of the interface between the aluminium alloy and ceramics, the XRD of Bruker-AXSD8AdvanceX was used in this study. To further observe and analyse the microstructure content and distribution of elements at the interface, a FEI Quanta 250F field-emission environment scanning electron microscope was used.

The equipment required for ceramic surface processing is a femtosecond laser system, model TH-FSLIS40, provided by Tianhong Laser Company. The experimental setup and principle are shown in Fig. 1b. The testing equipment boasts precise control over wavelength at 1035 nm, a top-of-the-line repetition rate of 1 MHz, maximum single pulse energy of 40 µJ, and a power range spanning from 0 to 40 W. Before conducting the femtosecond laser surface treatment, the samples underwent thorough preparation. Firstly, through ultrasonic cleaning with acetone and anhydrous ethanol, the material's surface was cleared of any grease or dust particles. Afterward, the material was carefully dried and securely fixed onto the sample table for processing. Olympus-OLS4100 laser confocal microscope was utilized to capture images of the machined Al_2O_3 ceramic surface.

Ceramic-aluminium alloy joints were brazed under

Table 1. Main composition of 7A52 aluminium alloy

element	Si	Fe	Cu	Mn	Mg	Zr	Zn	Ti	Al
wt.%	0.25	0.30	0.05–0.2	0.2–0.5	2.0–2.8	0.05–0.15	4.0–4.8	0.18	Bal

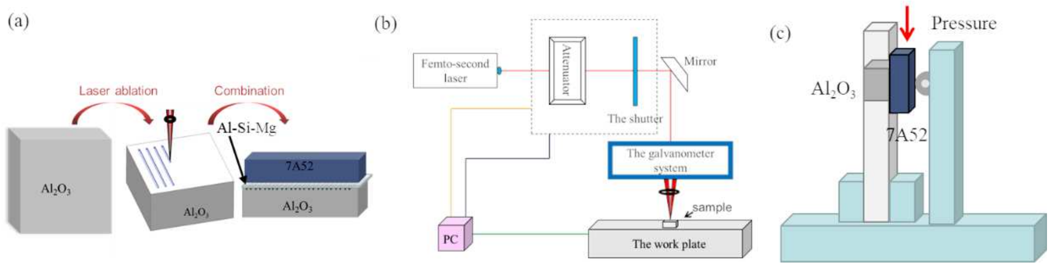

Figure 1. Femtosecond laser surface processing and brazing assembly diagram (a), femtosecond laser processing schematic diagram (b) and shearing schematic diagram (c)

vacuum conditions of 5×10^{-3} Pa using the same processing steps: temperature increase from room temperature to 500 °C at a rate of 5 °C/min with a dwell of 30 min, heating up to 610 °C at a rate of 3 °C/min with a dwell of 1 h, cooling down at a rate of 2 °C/min to 400 °C and natural cooling down to room temperature. The joint shear strength test was conducted at room temperature and the moving speed of the pressure head was 0.2 mm/min (Fig. 1c). The shear strength of each parameter was the average value of 3–4 samples.

III. Results and discussion

3.1. Femtosecond laser machining

The surface of Al_2O_3 ceramics has been machined using femtosecond laser technology, resulting in the creation of periodic structures with varying sizes and features depending on the scanning speeds and utilized processing paths. Figure 2 displays the machining schematic diagram and three-dimensional morphology of the resulting ceramic surface. As shown in Fig. 2a, the surface of the original ceramics is smooth. The Al_2O_3 surface was expertly machined with a femtosecond laser boasting a fixed power of 19 W, repetition rate of 1000 kHz, pulse width of 180 fs and a single pulse energy of 4.5 J/cm^2. The scanning interval was set to 75 µm, resulting in precise and accurate results. As shown in Fig. 2b, when the scanning speed is 1000 mm/s, the energy of the femtosecond laser is larger than the ablation threshold of the ceramic surface, and the periodic regular groove pattern can be machined on the ceramic surface. Upon reducing the scanning speed to 200 mm/s, as shown in Fig. 2c, it can be observed that as the scanning speed decreases, the heat input per unit area of the ceramic surface increases. Moreover, the width and depth of the laser-processed grooves also increase, even though the groove remains periodic. Constant scanning speed, introducing a cross pattern in the laser scanning path (as demonstrated in Fig. 2d), yields a micro-convex pattern on the Al_2O_3 surface. The area where the processing paths intersect shows deeper lesions. Table 2 displays the width and depth of the groove during the femtosecond laser processing cycle. It is evident that the average width of the periodic groove is 14.7 µm, while the depth is 9.5 µm at a scanning speed of 1000 mm/s, the ratio between width

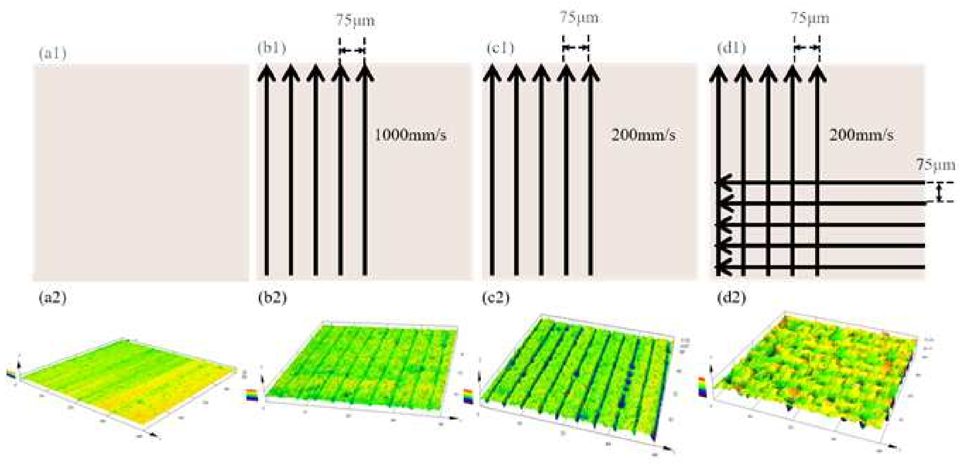

Figure 2. Schematic diagram of femtosecond laser machining of ceramic surfaces: a) original ceramics, b) shallow grooves, c) deep grooves and d) micro-convex platform

Table 2. Dimensions of grooves with different surface structures

Laser power [W]	Origin	Shallow groove	Deep groove	Micro-convex platform
Groove width [µm]	-	14.7	23.1	31.2
Groove depth [µm]	-	9.5	17.4	19.5
γ	-	1.5	1.3	1.6

and depth is approximately (the latter is commonly referred to as γ) 1.5, similar to shallow grooves. When the scanning speed decreases to 200 mm/s, the groove's width increases to approximately 23.1 µm, and its depth becomes approximately 17.4 µm due to the heightened heat input. This alteration creates a wide and profound groove shape, $\gamma \approx 1.3$, similar to deep grooves. The depth-width ratio exhibits a significant increase, and the reason behind it is attributed to the Gaussian pulse nature of the femtosecond laser. As the laser energy surpasses the ablation threshold of the ceramic surface, the heat input escalates, causing a noticeable increase in the depth. However, the widening of the area happens at a comparatively slower pace. When the scanning speed remains constant and the tool path becomes cross-interlaced, the width and depth of the groove increase. This is due to the fact that the same area of the ceramic surface is repeatedly exposed to the heat affected zone after being vertically machined and then horizontally machined, resulting in an improved laser energy absorption rate and enhanced laser ablation effect. The width has increased from 23.1 µm to an average of 31.2 µm, while the depth has increased to 19.5 µm, thus $\gamma \approx 1.6$.

Figure 3 depicts the contact angle between water and ceramics featuring varying surface structures. Upon testing with 1 µl of deionized water, it was observed that the average contact angle on the surface of the original ceramics is 55°. When the surface contains a shallow groove, the contact angle reduces from 55° to 22°. When the surface develops into a deep groove, the minimum contact angle decreases to a mere 18°, which gives the highest wettability of ceramic surfaces to water. It can be inferred that the surface structure created by femtosecond laser technique has a significant impact on enhancing the hydrophilicity of ceramic surfaces, elevating the surface tension of both solids and liquids, thus opening up new possibilities to enhance the solder and ceramics wettability. When employing a micro-convex structure, the contact angle may be reduced. This is due to the fact that the grooves on the ceramic surface are comparatively large and exhibit a narrow and deep morphology, which makes it difficult for the liquid to be fully filled. Consequently, this results in a larger contact angle between the ceramic surface and water. The Ra values of the ceramic surface before and after undergoing varied laser processing were found to be 0.5 ± 0.1, 2.17 ± 0.1, 3.16 ± 0.2 and 4.91 ± 0.5 µm, respectively.

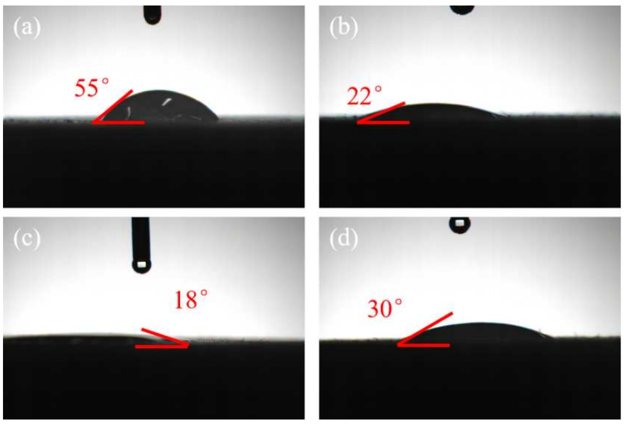

Figure 3. Contact angle of water on the surface of different ceramic periodic structures: a) original ceramic, b) shallow grooves, c) deep grooves and d) micro-convex platform

When Al_2O_3 ceramics are machined with a femtosecond laser, the surface roughness is significantly altered. This alteration has a positive impact on the enhancement of the ceramic surface wettability. On one hand, laser machining on ceramic surfaces creates grooves that increase the contact area for liquids, allowing for greater element diffusion. On the other hand, this process generates a multitude of micro and nanostructures on the surface [24], which can be seen in Fig. 4. This is likely to be the main reason behind the improved wettability of the ceramic surface.

3.2. Microstructure of Al_2O_3-7A52 brazed joint

By utilizing a femtosecond laser, a successful brazing was achieved between Al_2O_3 ceramics and 7A52 aluminium alloy with Al-Si-Mg brazing filler metal (Fig. 5). The brazing process was conducted at a temperature of 610 °C, pressure of 0.05 MPa and a holding time of 1 h. It is noteworthy that the solder will reach a full melting point of 610 °C. Furthermore, when subjected to pre-brazing pressure, the solder is capable of diffusing within the ceramic surface to establish a seamless and reliable interface, and there is clear evidence of reactant formation on the ceramic surface. With fem-

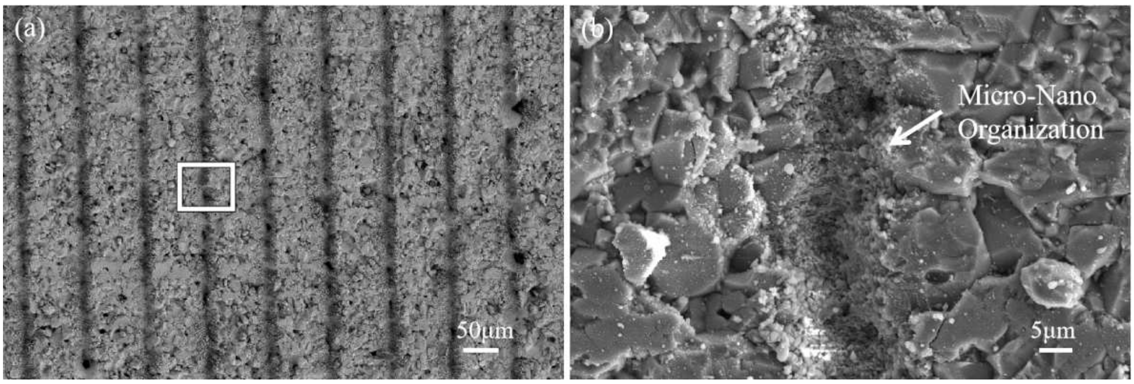

Figure 4. Microstructure of ceramic surface after femtosecond laser processing (a) and magnified micro-nanostructure (b)

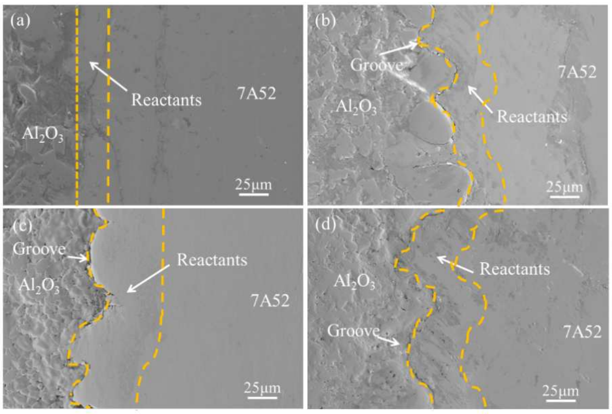

Figure 5. SEM diagram of Al_2O_3-7A52 aluminium alloy joint interface: a) original ceramics, b) shallow grooves, c) deep grooves and d) micro-convex platform

tosecond laser machining, the contact area between the ceramic surface and solder is dramatically improved, along with the discovery of abundant reaction products near the surface's periodic groove structure when using the same brazing parameters. Upon comparison of the reaction layers at the interface of the original planar ceramics and machined surfaces with solder, it is clear that the thickness of the reaction layer is significantly increased and that deeper grooves result in an even thicker reaction layer on the groove surface. The maximum thickness is achieved when utilizing a deep groove pattern.

To investigate the diffusion of elements at the joint interface of the Al_2O_3-7A52 aluminium alloy brazed joint, an element analysis was performed (Fig. 6). It has been discovered that the active component, magnesium, diffuses from the solder layer to both the ceramic and aluminium alloy sides, and the joint's characteristics primarily hinge on the solder and ceramic side reaction. The active Si element is primarily dispersed in the solder reaction layer, while some partial segregation still exists between Mg and Si. It is believed that Mg undergoes a reaction with Si during the diffusion process, resulting in the formation of Mg_2Si. This compound further aggregates and grows into larger plate shapes during the brazing process, negatively impacting the joint's properties due to its inherent brittleness [25].

When the femtosecond laser was applied to process the surface of Al_2O_3 ceramics, the distribution of interface elements in the joint can be observed in Fig. 7. It is apparent that, even though the periodic structure on the surface of the ceramics is relatively subtle, the integration between the ceramic surface and the initial flat ceramic and solder is more comprehensive compared to that of the initial planar ceramic and solder. As a result of this amalgamation, the reaction interface between the ceramic surface and solder results in an abundance of compounds being created along the grooved structure. Upon reviewing Figs. 6c and 7c, it was discovered that there is a higher concentration of the active element (Mg) in the surface reaction layer of ceramics with periodic grooves as opposed to the original planar ceramics. It has been demonstrated that the use of a periodic structure surface results in increased ceramic surface area and improved capillary action along the grooves. This subsequently enhances the reactivity with the active element Mg, leading to the formation of a more dependable reaction layer. With the increase of groove size, the thickness of the reaction layer formed by the reaction of ceramic surface active element Mg with Al_2O_3 becomes wider, as shown in Fig. 8. This phenomenon can be attributed to the effect of femtosecond laser, which leads to the increase in bonding area. As a result, the reduction of Al and O on the ceramic surface intensifies the wetting reaction at the interface between the solder and

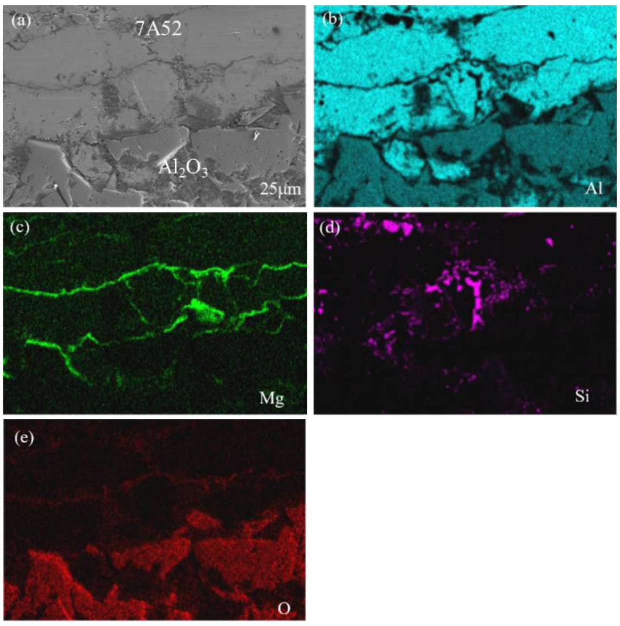

Figure 6. Microstructure and element distribution of original ceramics-7A52 brazed joint

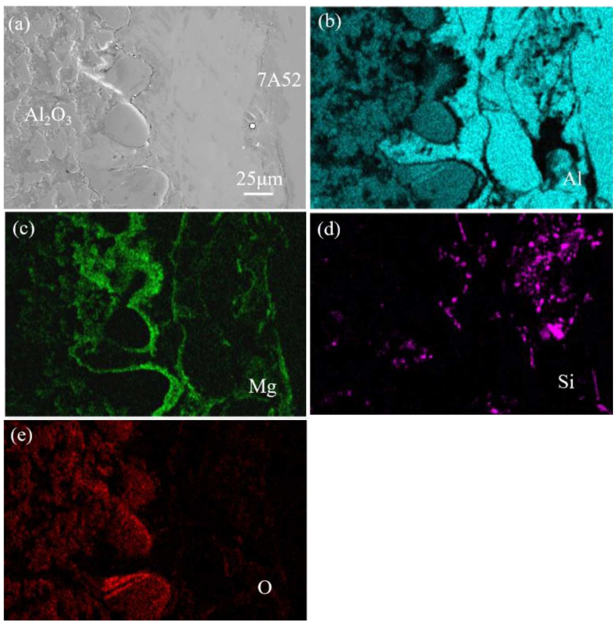

Figure 7. Microstructure and element distribution of Al_2O_3-7A52 brazed joint with shallow grooves structure

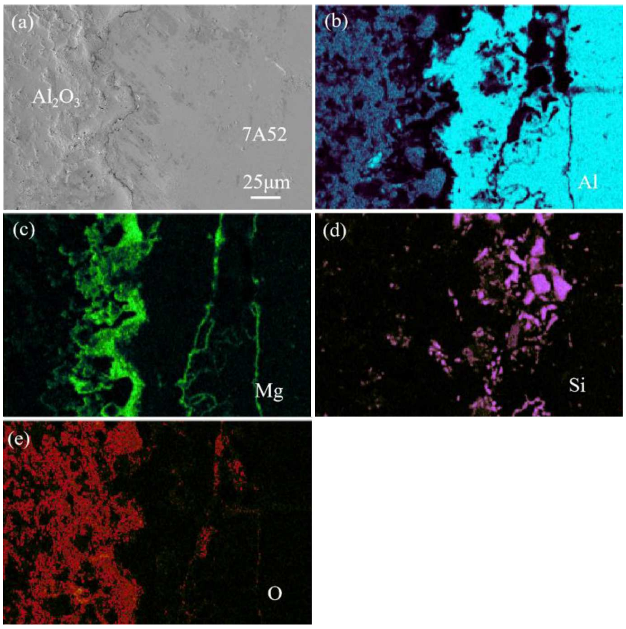

Figure 8. Microstructure and element distribution of Al_2O_3-7A52 brazed joint with micro-convex platform

ceramics, thereby facilitating the diffusion of Mg towards the ceramic side. The subsequent reaction with the ceramics results in the formation of spinel ($MgAl_2O_4$) and establishes a robust bond at the ceramic interface [26]. The chemical equation for this reaction is represented by the following formula:

$$Al_2O_3 + Mg \longrightarrow MgAl_2O_4 \tag{1}$$

In order to compare the diffusion of elements in the joint under different structures, an elemental analysis is conducted in the vicinity of the joint, as illustrated in Fig. 9. According to the line scanning results combined with the scanning path, the analysed material can be divided into three distinct regions. The first region, referred to as Zone I, is identified as the Al_2O_3 ceramic region. The second region, known as Zone II, represents the reaction zone between the solder and ceramic. Finally, Zone III corresponds to the aluminium alloy side of the sample.

It is evident from Fig. 10a that the thickness of the reaction layer ($MgAl_2O_4$) formed on the shallow groove surface measures approximately 30 μm. When the groove size increases, the intensity of the reaction between ceramic particles and Mg element in the solder also increases. This is due to the accumulation of magnesium near the surface of the periodic structure. These Mg atoms continually penetrate the ceramic particles, leading to the formation of a reaction layer. The capillary action exhibited on the surface of the periodic structure effectively "locks" the reaction layer at the interface, resulting in an increased thickness. The maximum attainable thickness is 40 μm, as visualized in Fig. 9b. By employing a micro-convex platform, the bonding effect between filler metal and ceramics can be diminished, subsequently weakening the reaction at the

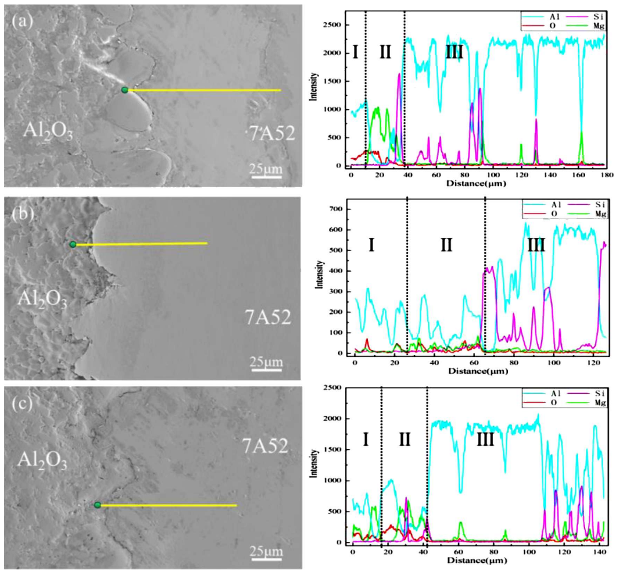

Figure 9. Diffusion of interface elements under different structures: a) shallow grooves, b) deep grooves and c) micro-convex platform

interface between ceramics and solder. Moreover, the reaction between Mg and Si elements and the ceramic surface is lessened as the spacing widens, resulting in a decrease in the thickness of reaction layer II from 40 to 25 μm. Unfortunately, the capillary effect and the "locking" effect generated by the groove structure are also reduced, contributing to a decrease in the bonding effect between ceramics and solder.

Figure 10 illustrates the strength of brazed joints between various ceramic periodic structures and 7A52 aluminium alloy, with the shear direction being perpendicular to the groove. Notably, the shear strength of ceramics-aluminium alloy brazed joints is significantly enhanced after femtosecond laser surface processing of Al_2O_3 ceramics. As the groove depth increases, the shear strength of the ceramics-7A52 aluminium alloy brazed joints also exhibits an increase from the origi-

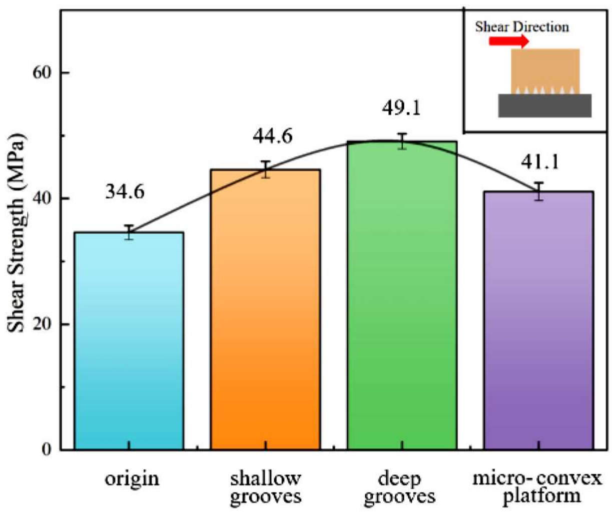

Figure 10. Shear strength comparison of brazed joints with various surface periodic structures

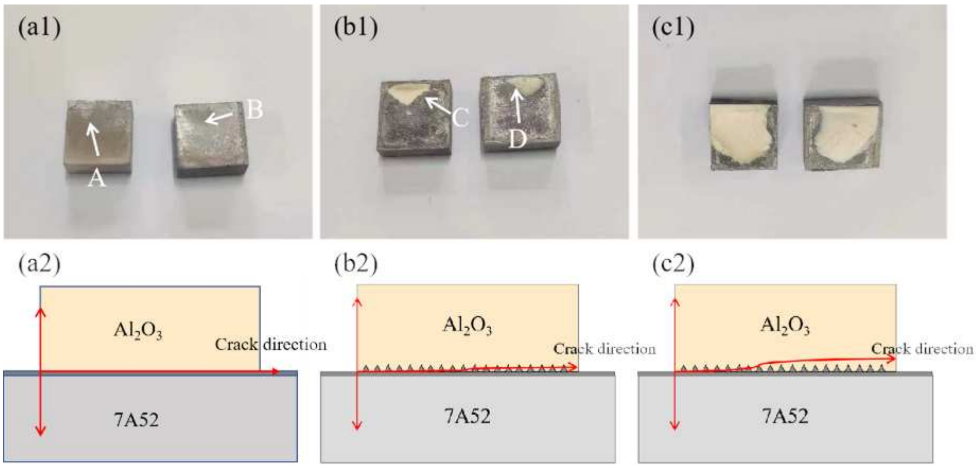

Figure 11. Fracture patterns of brazed joints in various structures: a) original ceramics, b) groove form and c) micro-convex platform

nal 34.6 to 49.1 MPa. However, it is important to note that when the surface structure features a micro-convex structure, the joint strength is relatively higher than the original. Nonetheless, it is comparatively lower than the shallow groove and deep groove structures, registering only 41.1 MPa.

Upon examination of the fracture pattern in the joint, it becomes apparent that the Al_2O_3-7A52 aluminium alloy brazed joint can be classified into two distinct categories: i) fractures that occur along the brazing interface and ii) fractures that originate at the beginning of the brazing interface and extend all the way to the ceramic interface (Fig. 11). After brazing the Al_2O_3-7A52 aluminium alloy, it is observed that the joint fractures at the interface between the ceramics and aluminium alloy. Figure 12 depicts the interface reaction products that can be found on the surface of the ceramics. On one side of the aluminium alloy Fig. 12b reveals a distinct absence of any ceramic particles, and instead showcases the tell-tale signs of brittle fracture steps that stem from solder tearing and damaging the aluminium alloy body. During the shear test of the laser surface machined Al_2O_3-7A52 aluminium alloy brazed joint, it was observed that the fracture begins at the interface and then the crack changes its direction to propagate into the ceramics under the influence of grooves. This is also one of the factors contributing to the increase in shear strength. Upon microscopic analysis of the fracture near the point of crack propagation direction change, it was observed that the grooves on the ceramic surface were completely filled with reaction layer products of solder and ceramics, as exemplified in Fig. 12c and Table 3. From Fig. 12d, ceramic particles were discovered adhered to one side of the aluminium alloy surface. In order to provide additional validation of the reaction products at the brazed joint, XRD composition analysis was

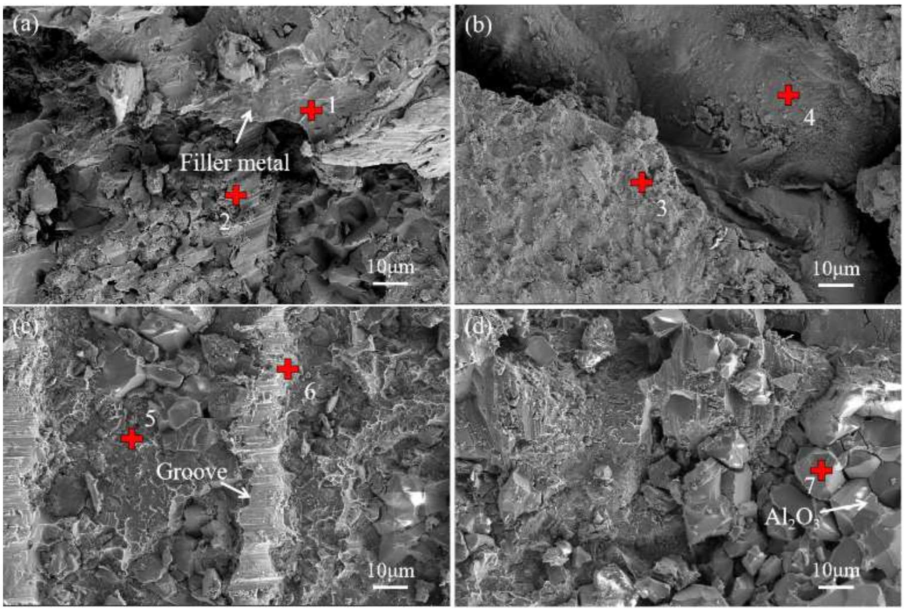

Figure 12. Fracture morphology of brazed joints: a) original ceramic side fracture, b) aluminium alloy side fracture, c) deep groove ceramic side fracture and d) deep groove ceramic brazing aluminium alloy side fracture

Table 3. Content of elements at each point of the break in Fig. 12

	Al	Si	Mg	O	Possible phase
1	42.34	4.59	13.26	39.81	Mg_2Si, $Mg(Al_2O_4)$
2	82.97	2.33	7.84	6.86	Al-Si-Mg, Mg_2Si
3	81.64	3.27	5.84	9.25	Al-Si-Mg, Mg_2Si
4	94.81	0.36	1.06	3.77	α-Al, 7A52
5	79.45	2.05	9.88	8.62	Al-Si-Mg, Mg_2Si
6	62.16	2.53	12.34	22.97	Mg_2Si, $Mg(Al_2O_4)$
7	65.21	0.00	0.00	34.79	Al_2O_3

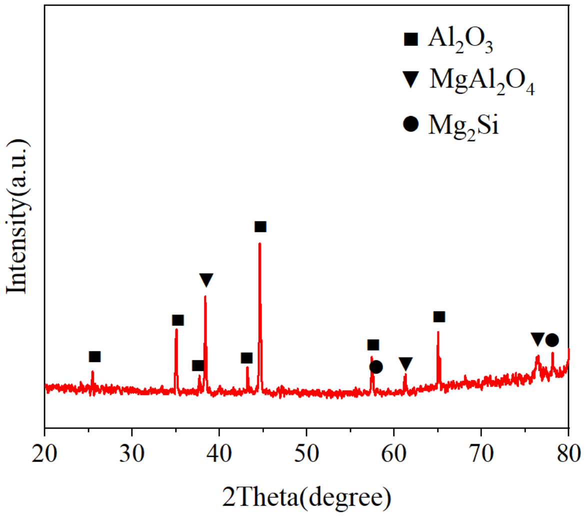

Figure 13. XRD pattern of the brazing joint between deep groove ceramics and aluminium alloy

conducted on the fracture interface of the brazed joint with a deep groove structure (Fig. 13). The results from this analysis serve to further confirm the presence of reaction products at the joint.

The principle diagram of the enhancement mechanism of alumina ceramics machined by femtosecond laser is illustrated in Fig. 14. During the direct brazing process, the inherent ceramic surface can impede the active elements from effectively penetrating the ceramic pores. As a result, the majority of Mg and Si active elements become trapped between the interlayer and the ceramic surface, rendering them unable to interact with additional alumina particles. This, in turn, leads to inadequate diffusion reaction between the solder layer and the base metal - a critical factor contributing to the low strength of direct brazing joints between 7A52 aluminium alloy and alumina ceramics. High-intensity laser ablation was used with femtosecond laser to puncture the surface of alumina ceramics (Fig. 14b). As a result, more active elements in the solder layer are able to pass through the ceramic pores and react with alumina particles, further enhancing the reaction. Simultaneously, the ceramic surface exposes a greater quantity of alumina particles, thereby enhancing the contact area between active elements and ceramic particles. This heightened interaction promotes a more comprehensive diffusion reaction between the solder layer and base metal. This finding is further supported by the augmented thickness of the reaction layer depicted in Fig. 8, which was brought about with the assistance of femtosecond laser technology. Compared to direct brazing techniques, femtosecond laser processed ceramics exhibit enhanced bonding properties due to a more complete reaction at the interface. Under similar conditions of reaction time and pressure, the reaction between active element Mg and alumina particles is significantly enhanced, leading to the formation of a greater quantity of reaction products ($MgAl_2O_4$). As a result, the formation and segregation of the Mg_2Si phase is significantly reduced. Overall, these improvements contribute to stronger and more reliable joint bonds.

IV. Conclusions

Femtosecond laser was utilized to create various periodic structures on the surface of Al_2O_3 ceramics, resulting in a significant enhancement of the shear strength of ceramics-aluminium alloy brazed joints. The following conclusions are obtained:

(1) The surface of Al_2O_3 ceramics was skillfully machined using a powerful femtosecond laser. This laser had a fixed power of 19 W, a repetition rate of 1000 kHz,

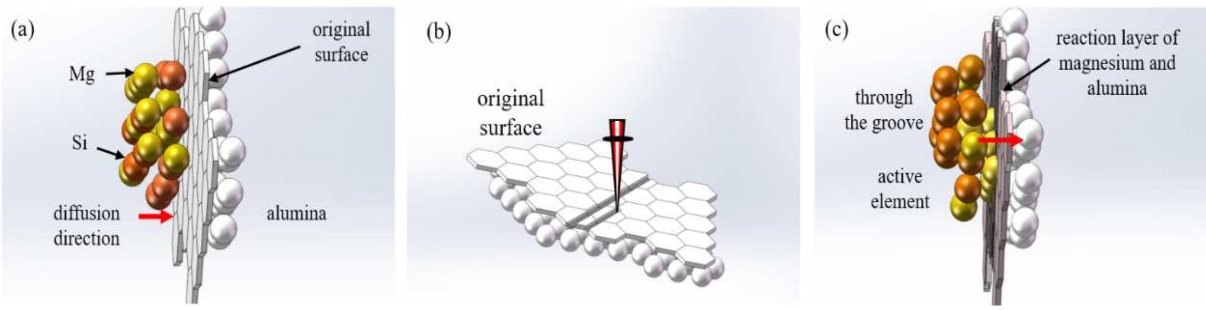

Figure 14. Schematic diagram of diffusion enhancement mechanism for femtosecond laser-assisted machining of ceramics

a pulse width of 180 fs and a single pulse energy of 4.5 J/cm^2. To ensure precision, the scanning interval was set at 75 μm, and the scanning speed was set to 1000 mm/s, 200 mm/s for linear and 200 mm/s for cross-scanning. In this way it is possible to fabricate shallow grooves, deep grooves and micro-convex platform on the surface of Al_2O_3 ceramics.

(2) The formation of a periodic structure on the surface of the Al_2O_3 ceramics leads to an increase in the thickness of the reaction layer ($MgAl_2O_4$) in the brazed joint. In particular, the thickness of the reaction layer varies depending on the depth of the groove or the presence of micro-protuberances. For shallow grooves, the reaction layer thickness was 25 μm, while for deep grooves it was 40 μm. In the case of micro-convex platform, the thickness was 30 μm. Correspondingly, the shear strength of the joints also varies (44.6, 49.1 and 41.1 MPa), respectively. It is noteworthy that these values represent a significant improvement compared to the original planar ceramics-aluminium alloy joint (i.e. increase of shear strength of 29%, 42% and 19%).

(3) Femtosecond laser machining of Al_2O_3 ceramics results in the creation of a periodic structure, which significantly alters the surface roughness of the ceramics. This alteration has a positive impact on the wettability of the ceramics. Firstly, the surface structure modification of ceramics increases the contact area between the solder and ceramics, thereby enhancing the diffusion reaction between them. This ultimately facilitates the reaction between the active element Mg and Al_2O_3 ceramic particles, leading to the formation of $MgAl_2O_4$ spinel. Consequently, this enhances the joint formation between the solder and ceramics. Additionally, the periodic groove structure created during the machining process influences the direction of crack propagation and acts as a crack resistance mechanism.

References

1. A. Serjouei, G. Gour, X. Zhang, S. Idapalapati, G. Tan, "On improving ballistic limit of bi-layer ceramic-metal armor", *Int. J. Impact Eng.*, **105** (2017) 54–67.
2. H.R. Hwang, R.Y. Lee, "The effects of metal coating on the diffusion bonding in Al_2O_3/Inconel 600 and the modulus of rupture strength of alumina", *J. Mater. Sci.*, **31** (1996) 2429–2435.
3. M.B. Uday, M.N. Ahmad Fauzi, H. Zuhailawati, A.B. Ismail, "Evaluation of interfacial bonding in dissimilar materials of YSZ-alumina composites to 6061 aluminium alloy using friction welding", *Mater. Sci. Eng. A*, **528** [3] (2011) 1348–1359.
4. H. Hao, Z. Jin, X. Wang, "The influence of brazing conditions on joint strength in Al_2O_3/Al_2O_3 bonding", *J. Mater. Sci.*, **29** (1994) 5041–5046.
5. M. Kobashi, T. Ninomiya, N. Kanetake, T. Choh, "Effect of alloying elements in the brazing sheet on the bonding strength between Al_2O_3 and aluminium", *Scripta Mater.*, **34** [3] (1996) 415–420.
6. X. Si, J. Cao, X. Song, Y. Qu, J. Feng, "Reactive air brazing of YSZ ceramic with novel Al_2O_3 nanoparticles reinforced Ag-CuO-Al_2O_3 composite filler: Microstructure and joint properties", *Mater. Design.*, **114** (2017) 176–184.
7. M. Ksiazek, B. Mikulowski, M. Richert, "Effect of Nb plus Ti coating on the wetting behavior, interfacial microstructure, and mechanical properties of Al/Al_2O_3 joints", *J. Mater. Sci.*, **45** [8] (2010) 2194–2202.
8. A.Y. Vorobyev, C. Guo, "Laser makes silicon superwicking", *Optics Photonics News*, **21** [12] (2010) 38.
9. Y. Zhang, G. Zou, L. Liu, A. Wu, Z. Sun, Y.N. Zhou, "Vacuum brazing of alumina to stainless steel using femtosecond laser patterned periodic surface structure", *Mater. Sci. Eng. A*, **662** (2016) 178–184.
10. Z. Lin, M. Hong, "Femtosecond laser precision engineering: From micron, submicron, to nanoscale", *Ultrafast Sci.*, **2021** (2021) 9783514.
11. P. van Assenbergh, E. Meinders, J. Geraedts, D. Dodou, "Nanostructure and microstructure fabrication: from desired properties to suitable processes", *Small*, **14** [20] (2018) 1703401.
12. E. Pomerantseva, F. Bonaccorso, X. Feng, Y. Cui, Y. Gogotsi, "Energy storage: The future enabled by nanomaterials", *Science*, **366** [6468] (2019) eaan8285.
13. J. Bonse, S. Höhm, S.V. Kirner, A. Rosenfeld, J. Krüger, "Laser-induced periodic surface structures (LIPSS) - A scientific evergreen", paper STh1Q.3 in *Conference on Lasers and Electro-Optics*, OSA Technical Digest, Optica Publishing Group, 2016.
14. F.A. Müller, C. Kunz, S. Gräf, "Bio-inspired functional surfaces based on laser-induced periodic surface structures", *Materials*, **9** [6] (2016) 476.
15. J. Bonse, S.V. Kirner, S. Höhm, N. Epperlein, D. Spaltmann, A. Rosenfeld, J. Krüger, "Applications of laser-induced periodic surface structures (LIPSS)", pp. 114–122 in: *Laser-based Micro-and Nanoprocessing*, XI SPIE, 2017.
16. C. Kunz, J. Bonse, D. Spaltmann, C. Neumann, A. Turchanin, J.F. Bartolomé, F.A. Mueller, S. Graef, "Tribological performance of metal-reinforced ceramic composites selectively structured with femtosecond laser-induced periodic surface structures", *Appl. Surface Sci.*, **499** (2020) 143917.
17. C.-Y. Chen, C.-J. Chung, B.-H. Wu, W.-L. Li, C.-W. Chien, P.-H. Wu, C.-W. Cheng, "Microstructure and lubricating property of ultra-fast laser pulse textured silicon carbide seals", *Appl. Phys. A*, **107** (2012) 345-350.
18. L. Ji, X. Lv, Y. Wu, Z. Lin, Y. Jiang, "Hydrophobic light-trapping structures fabricated on silicon surfaces by picosecond laser texturing and chemical etching", *J. Photon. Energy*, **5** [1] (2015) 053094–053094.
19. Y. Zhao, Y. Su, X. Hou, M. Hong, "Directional sliding of water: biomimetic snake scale surfaces", *Opto-Electron. Adv.*, **4** [4] (2021) 210008.
20. A.Y. Vorobyev, C. Guo, "Laser turns silicon superwicking", *Optics Express*, **18** [7] (2010) 6455–6460.
21. R. Jagdheesh, "Fabrication of a superhydrophobic Al_2O_3 surface using picosecond laser pulses", *Langmuir*, **30** [40] (2014) 12067–12073.
22. N. Chen, B. Chen, D. Liu, Y. Song, H. Zhu, X. Song, C. Tan, "Joining of nanosecond laser irradiation modified-AlN and Cu", *Ceram. Int.*, **47** [19] (2021) 27979–27986.
23. H.Y. Chen, X.C. Wang, L. Fu, M.Y. Feng, "Effects of surface microstructure on the active element content and wetting behavior of brazing filler metal during brazing

Ti_3SiC_2 ceramic and Cu", *Vacuum*, **156** (2018) 256–263.
24. A.Y. Vorobyev, C. Guo, "Direct femtosecond laser surface nano/microstructuring and its applications", *Laser Photon. Rev.*, **7** [3] (2013) 385–407.
25. T. Yang, D. Zhang, K. Wang, J. Huang, "Aluminium-silicon-magnesium filler metal for aluminium vacuum brazing wettability and characteristics of brazing microstructure", *Mater. Trans.*, **57** [6] (2016) 983–987.
26. D. Zhang, X. Qian, X. Li, K. Wang, "Effect of vacuum heat treatment on microstructures and mechanical properties of 7A52 aluminum alloy-Al_2O_3 ceramic brazed joints", *Front. Mater.*, **8** (2021) 634658.